

X-ray absolute calibration of the time response of a silicon photodiode

John F. Seely, Craig N. Boyer, Glenn E. Holland, and James L. Weaver

The time-dependent response of a 1-mm² silicon photodiode was characterized by use of pulsed synchrotron radiation in the 4- to 16-nm-wavelength range. Modeling the input radiation pulse and the electrical response of the photodiode allowed the photodiode's capacitance as a function of wavelength and applied bias voltage to be determined. The capacitance was in the 7- to 19-pF range and resulted in response fall times as small as 0.4 ns. The capacitance determined by pulsed x-ray illumination was in good agreement with the capacitance determined by pulsed optical laser illumination. The absolute responsivity was measured by comparison with the responsivity of a calibrated photodiode. © 2002 Optical Society of America

OCIS codes: 040.7480, 040.5160, 040.6040, 230.5170.

1. Introduction

Silicon p-n junction photodiodes with small sensitive areas and fast response times have been used to record the x-ray and the extreme ultraviolet (EUV) radiation from laser-produced plasmas and other transient radiation sources.^{1,2} The photodiodes have a thin (≤ 6 nm) SiO₂ surface dead layer that results in high x-ray and EUV responsivity, small areas (≤ 1 mm²), low capacitance, and subnanosecond rise and fall times.³

Although silicon p-n junction photodiodes are widely used for the measurement of absolute radiation fluxes in the x-ray and EUV ranges,³ the time response has not been previously studied with pulsed synchrotron radiation. The objective of performing this research is to characterize the time response of a 1-mm² photodiode by use of subnanosecond pulses of synchrotron radiation in the 4- to 16-nm-wavelength range.

Modeling the input radiation pulse and the electrical response of the photodiode and the measurement apparatus allowed the photodiode's capacitance,

which affects the speed of the device, to be determined as a function of the incident x-ray wavelength and the applied bias voltage. The photodiode's capacitance also was determined by use of pulsed optical laser illumination and was in good agreement with the capacitance determined by x-ray illumination. The steady-state responsivity of the 1-mm² photodiode was compared with the responsivity of an absolutely calibrated 1-cm² reference photodiode.

2. Pulsed X-ray and Laser Illumination

The x-ray measurements were performed at the Naval Research Laboratory beamline X24C at the National Synchrotron Light Source (NSLS) at Brookhaven National Laboratory. A monochromator provided dispersed x-ray and EUV radiation with a resolving power of 600.^{4,5} Thin metal filters attenuated the higher harmonics from the monochromator while passing the x-ray or the EUV bandpass of interest. Removal of the metal filter and setting the monochromator grating to the zero diffraction order allowed the photodiode to be illuminated by broadband radiation consisting of all wavelengths greater than approximately 1 nm.

The NSLS storage ring operated in single electron-bunch mode with 2.8-GeV energy, a bunch period of 567 ns, and a maximum current of 75 mA after refill of the storage ring.⁶ The ring current decreased slowly over a period of 12 h at which time the storage ring was refilled. Additional data were recorded with a 25 electron-bunch mode with 2.5-GeV energy and 260-mA maximum ring current equally distributed in the 25 electron bunches. The 567-ns orbital

J. F. Seely (john.seely@nrl.navy.mil) and J. L. Weaver are with the Naval Research Laboratory, Code 7674, 4555 Overlook Avenue SW, Washington, DC 20375-5352. C. N. Boyer is with Universities Space Research Associates, 300 D Street SW, Washington, DC 20024. G. E. Holland is with SFA Incorporated, 9315 Largo Drive, West Suite 200, Largo, Maryland 20774.

Received 3 January 2002; revised manuscript received 15 May 2002.

0003-6935/02/255209-09\$15.00/0

© 2002 Optical Society of America

Table 1. Photodiode Types, Sensitive Areas, and Apertures

Number	Type	Area (mm ²)	Aperture Diameter (mm)
1	AXUV-HS5	1 × 1	0.8
2	AXUV-HS5	1 × 1	0.4
3	AXUV-HS1	0.22 × 0.22	0.15
4	AXUV-100G	10 × 10	0.8

period consisted of 25 electron-bunch intervals and 5 intervals with no electrons. Thus in the 25 electron-bunch mode, the electron-bunch separation time was 18.9 ns.

The separation times between electron bunches in the 25 bunch mode (18.9 ns) and in the single bunch mode (567 ns) were much longer than the duration of the transient signals from the photodiodes. On the basis of the observed oscilloscope traces, the pulses from individual electron bunches in a sequence were essentially the same. This allowed the summation and averaging of a large number (typically 100) of oscilloscope traces to improve the signal-to-noise ratio in the cases in which the signal was rather low owing to weak incident radiation intensity or a small aperture over the photodiode.

According to previous characterizations by the NLS facility,⁶ the radiation pulse from an electron bunch circulating in the NLS storage ring is approximately Gaussian in shape. The full width at half-maximum (FWHM) duration of the pulse weakly depends on the ring current and is typically 0.6 ns.

As listed in Table 1, photodiodes (International Radiation Detectors Inc.,⁷ Torrance, California) with various sensitive areas were mounted on a translational fixture so that a selected photodiode could be moved into the radiation beam. Small apertures were mounted just above the photodiode surface. In each case, the aperture limited the illumination to an area smaller than the sensitive area of the photodiode. The diameter of the radiation beam incident on the photodiodes was approximately 2 mm and overfilled the apertures.

The p-n junction photodiodes were fabricated with a lithographic process.⁷ Each photodiode consisted of a top SiO₂ dead layer approximately 6 nm thick, an underlying n-type (phosphorous doped) region approximately 100 nm thick, a p-type (epitaxial) region 30 to 40 μm thick, and a 500 μm p+ substrate. The dark current (without illumination) per sensitive area was less than 1 pA/cm².

The photodiodes with areas ≤ 1 mm² were mounted on 50-Ω, high-bandpass coaxial cables. The cables and vacuum feedthroughs were tested with a subnanosecond pulse generator and a 1-GHz oscilloscope with 5 gigasamples/s, and the cables and feedthroughs did not significantly alter the signal pulses. The photodiodes with 1-cm² areas were mounted on 50-Ω, low-bandpass coaxial cables.

The time-averaged current from the selected photodiode (of each type with sensitive area 1 cm², 1 mm², or smaller) was recorded by a Keithley-type 617

electrometer without bias voltage applied to the photodiode. In addition, the time-averaged currents from the photodiodes with areas ≤ 1 mm² were recorded by a Keithley 237 electrometer (Keithley Instruments Inc., Cleveland, Ohio) with bias voltage applied to the photodiode. The top surface of the photodiode was grounded, and the current was drawn from the lower portion of the photodiode, the p-type region. The two electrometers were cross calibrated in the unbiased mode under the same illumination and cabling conditions, and the Keithley 237 measurements were found to be smaller than the Keithley 617 measurements by a factor of 1.125. This correction factor was applied during comparison of the time-averaged currents measured by the two electrometers.

The transient photodiode signal was recorded with a reverse bias voltage and 50-Ω, high-bandpass coaxial cabling. The pulse was inverted by a bias tee, Picosecond Pulse Labs Model 5530A (Boulder, Colorado). The reverse bias voltage could be adjusted to one of four values: 22, 44, 66, or 88 V. The pulse was amplified by a voltage signal amplifier (Femto Inc. Model DUPVA-1-70, Berlin, Germany) and was recorded by an oscilloscope (Tektronix Model TDS684B, Beaverton, Oregon). The amplifier had a 1-GHz bandpass and a 680 gain that were measured with a precision attenuator and a nanosecond pulse generator. The oscilloscope had a 1-GHz passband (when its vertical sensitivity was ≥ 10 mV/division) and 5 gigasamples/s. The oscilloscope was triggered by a probe mounted in the storage ring that sensed the changing current (dI/dt) as an electron bunch passed near the probe.

In reverse-bias mode, the positive voltage was applied to the top portion of the photodiode, the n-type region, and the negative voltage was applied to the lower p-type region. The applied electric field was in the same direction as the built-in electric field in the depletion region and tended to oppose electron-hole diffusion across the junction. This maintained the low dark current (< 1 pA/cm²) while rapidly sweeping out the charge created in the depletion region by the deposition of radiation energy. In addition, a reverse-bias voltage tends to increase the width of the depletion region, which has the beneficial effect of reducing the capacitance and increasing the speed of the device.⁸

The time dependence of the photodiode signals recorded under various illumination conditions are shown in Fig. 1. The curves are averages of typically 100 pulses recorded by the oscilloscope. The peak signals are normalized to unity in Fig. 1. The curve labeled HS1 0-mono is the signal from an AXUV-HS1 photodiode with a 0.15-mm-diameter aperture (photodiode number 3 in Table 1) illuminated by the zero-order radiation from the monochromator. The reverse-bias voltage was 44 V. The photodiode's small sensitive area (0.22 mm × 0.22 mm) and high-bandpass cable mount results in characteristic rise and fall times of 0.25 ns.⁷ The signal from this photodiode, the curve labeled HS1 0-mono in Fig. 1, is

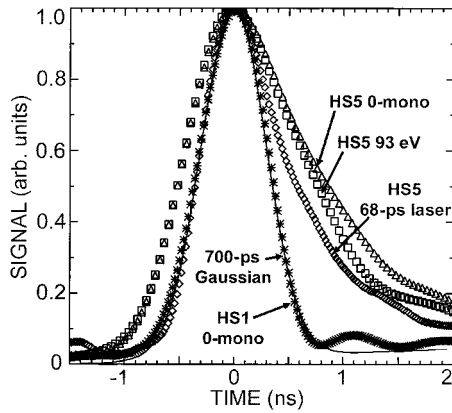


Fig. 1. Signals measured by means of pulsed x-ray and laser illumination. The curve labeled HS1 0-mono (asterisk data symbols) was recorded by the AXUV-HS1 photodiode with a 0.15-mm-diameter aperture and was illuminated by the monochromator's zero-order radiation. A 700-ps Gaussian curve is fitted to the data points. The other three curves were recorded by means of the AXUV-HS5 photodiode with a 0.8-mm-diameter aperture. The data symbols and the illumination conditions are HS5 0-mono (triangular: zero-order radiation), HS5 93 eV (square; 93-eV radiation), and HS5 68-ps laser (diamond; 68-ps pulsed laser radiation).

considered a good representation of the shape of the radiation pulse from the synchrotron. As shown in Fig. 1, this signal is modeled very well by a Gaussian with 0.7-ns FWHM. Considering the characteristic rise and fall times of the AXUV-HS1 photodiode and the 1-GHz bandpass of the amplifier and the oscilloscope, the observed 0.7-ns FWHM Gaussian is consistent with the 0.6-ns FWHM Gaussian radiation pulse shape that was determined by the NSLS facility.

The curves labeled HS5 0-mono and HS5 93 eV in Fig. 1 are the signals recorded by an AXUV-HS5 photodiode with a 0.8-mm aperture (photodiode 1 in Table 1) and with illumination by the zero-order beam or the 93-eV beam from the monochromator, respectively. The reverse bias voltage was 88 V. The 1-mm² AXUV-HS5 photodiode has a larger capacitance than the smaller AXUV-HS1 photodiode, and this increased capacitance results in significantly longer fall times as seen in Fig. 1.

The curve labeled HS5 68-ps laser in Fig. 1 was recorded by the AXUV-HS5 photodiode with a 0.8-mm aperture (photodiode 1 in Table 1) and illuminated by the 68-ps pulse from a diode laser (wavelength 670 nm). The reverse-bias voltage was 88 V. Compared with the AXUV-HS5 signals with synchrotron radiation illumination, the AXUV-HS5 signal with short-pulse laser illumination has faster rise and fall times, and these faster times result from the more transient driving pulse as is discussed in Section 3.

3. Signal Analysis

Modeling the input radiation pulse and the electrical response of the photodiode and the measurement ap-

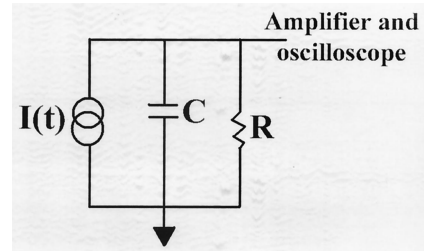


Fig. 2. Electrical circuit for the photodiode. $I(t)$ represents the time-dependent current resulting from the transient deposition of radiation energy in the depletion region.

paratus allowed the photodiode capacitance to be determined. The photodiode was modeled with the electrical circuit shown in Fig. 2. Neglecting the effects of the amplifier and oscilloscope bandpasses, the circuit equation is

$$CdV/dt + V(t)/R = I(t), \quad (1)$$

where C is the photodiode capacitance and $R = 50 \Omega$. The input current pulse $I(t)$ is assumed to be Gaussian, the same as the radiation driving pulse, since the generation of charge carriers by the incident radiation is fast compared with the response time of the photodiode. Setting

$$I(t) = I_o \exp[-(t - t_o)^2/\sigma^2],$$

where I_o is the peak value at time t_o and σ is the width of the input pulse, the solution to Eq. (1) may be written

$$V(t) = (I_o/C) \exp(-t/\tau) \int^t f(t') dt', \quad (2)$$

where $\tau = RC$ and $f(t') = \exp[-(t' - t_o)^2/\sigma^2] \exp(t'/\tau)$.

Let us assume that the amplifier has gain G_1 and a single high-frequency pole $f_1 = 1/2\pi\tau_1$ and that the oscilloscope has vertical sensitivity G_2 and a high-frequency pole $f_2 = 1/2\pi\tau_2$. Then the amplified voltage pulse recorded by the oscilloscope, including the effects of the amplifier and oscilloscope bandpasses, may be written⁹

$$V(t) = (I_o/C)(G_1 G_2/\tau_1 \tau_2) \exp(-t/\tau_2) \int^t \left\{ \exp(-v/\tau_1) \times \int^v \left[\exp(-u/\tau) \int^u f(t') dt' \right] \times \exp(u/\tau_1) du \right\} \exp(v/\tau_2) dv. \quad (3)$$

The effects of the amplifier and the oscilloscope on the signal, with characteristic times τ_1 and τ_2 , are analogous to the effect of the photodiode characteristic time τ in Eq. (2).

The measured voltage pulse is a function of three unknown parameters: I_o (peak value of the input pulse), t_o (time of the peak input pulse), and C (pho-

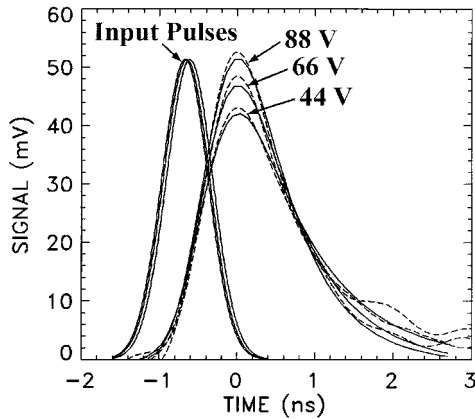


Fig. 3. Observed voltage pulses (dashed curves) and the fitted voltage pulses (solid curves) recorded with the AXUV-HS5 with a 0.8-mm aperture, 13.3-nm incident radiation, and bias voltages of 88, 66, and 44 V. The inferred input pulses are also shown.

todiode capacitance). The other parameters R , G_1 , τ_1 , G_2 , τ_2 , and σ are known. Determination of the three unknown parameters was accomplished by fitting Eq. (3) to the measured oscilloscope curves by use of the least-squares technique.

The data were recorded with the AXUV-HS5 with a 0.8-mm aperture (photodiode 1 in Table 1), incident radiation pulses in the 4.8- to 16.5-nm-wavelength range, and reverse-bias voltages of 44, 66, and 88 V. For wavelengths shorter than 4.8 nm, the incident radiation intensity was too low to produce a usable transient signal. The measured voltage signal pulses, fitted voltage pulses, and inferred input pulses for the case of 13.3-nm incident radiation are shown in Fig. 3. For display purposes, the signal curves were shifted in time so that their peak values occurred at zero time.

For each illumination condition (incident wavelength and bias voltage), the fitted value of the area under the curve, the curve height, the capacitance C , and the offset time t_o are shown in Fig. 4. The areas shown in Fig. 4(a) and the curve heights shown in Fig. 4(b) vary with the incident radiation intensity. Within the uncertainties of the fits to the curves, for a particular wavelength, the areas do not vary significantly with bias voltage, whereas the curve heights increase with bias voltage (see also Fig. 3). The heights tend to increase with bias voltage, and the durations of the transient signals tend to decrease with bias voltage, thus conserving the area. Since the signal fall time is primarily a function of the photodiode's capacitance, this conservation implies that the capacitance decreases with bias voltage.

The values of capacitance inferred from the least-squares fitting are shown in Fig. 4(c). Within the uncertainty in the measurements, we conclude that the capacitance values decrease with bias voltage, are approximately independent of the incident wavelength, and are in the range of 7 to 19 pF for applied bias voltages of 44 to 88 V.

The fitted values of the offset time t_o , the time

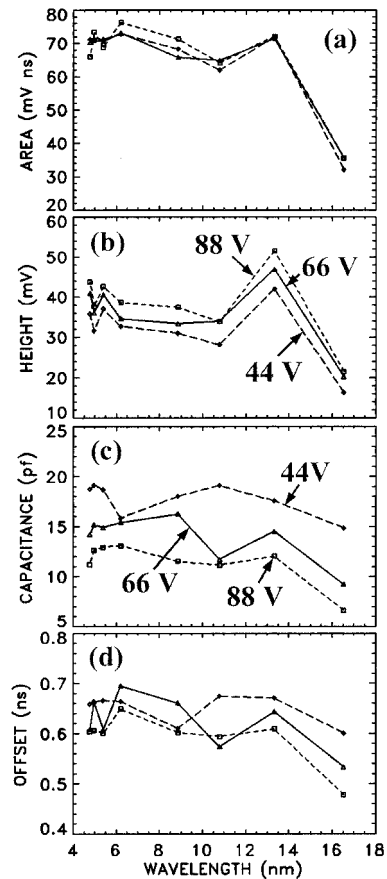


Fig. 4. Fitted parameters for the AXUV-HS5 photodiode with a 0.8-mm aperture and x-ray illumination. (a) Area under the voltage signal curve. (b) Height of the voltage signal curve. (c) Photodiode capacitance. (d) Offset time between the peaks of the signal curve and the driving pulse.

between the peak of the input radiation pulse and the peak of the measured transient signal, are shown in Fig. 4(d). Within the uncertainty in the measurements, the offset time is approximately independent of the bias voltage and the incident wavelength. Modeling indicates that the offset time depends primarily on the width of the input synchrotron radiation pulse (which is approximately 0.6-ns FWHM and is constant), the rise times of the amplifier and oscilloscope (which are constants), and the intrinsic photodiode rise time.

The rise times of the signals shown in Fig. 3 from the AXUV-HS5 photodiode (photodiode 1 in Table 1) are approximately 0.4 ns. Similarly, the rise times of the curves (from the 25% to the 75% levels) in Fig. 1 labeled HS5 93 eV and HS5 0-mono, also from the AXUV-HS5 photodiode with synchrotron radiation illumination, are 0.4 ns. For the case of illumination by the 68-ps laser, the curve labeled HS5 68-ps laser in Fig. 1 has a rise time of 0.25 ns. The AXUV-HS1 photodiode (photodiode 3 in Table 1), with a smaller sensitive area and capacitance, also has a 0.25-ns rise time for synchrotron radiation illumination (see the curve labeled HS1 0-mono in Fig. 1).

Thus, in general, the signal rise time is determined

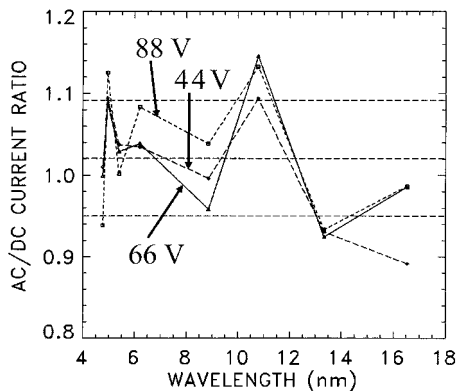


Fig. 5. Ratio of the equivalent current from the AXUV-HS5 photodiode measured in the transient mode and the steady-state current measured by the Keithley 237 electrometer. The horizontal dashed lines indicate the average and the standard deviation values.

primarily by the duration of the input driving pulse and the bandpass of the measurement apparatus and is relatively insensitive to the photodiode capacitance. By comparing the fall times of the curves in Fig. 1, it is apparent that the fall time is determined primarily by the photodiode capacitance. The different sensitivities of the signal curve shape, in particular the rise and the fall time, to the curve parameters allowed for an accurate least-squares fit to the measured signal curves with three unknowns (I_o , t_o , and C). In the case of slower photodiodes than studied here, the effect of capacitance on the signal rise time would become relatively more important.

The ratio of the equivalent current from the AXUV-HS5 photodiode measured in transient mode and the steady-state current measured by the Keithley 237 electrometer is shown in Fig. 5. The equivalent transient current is the integrated area under the oscilloscope curve shown in Fig. 4(a) divided by the amplifier gain (680), the resistance (50 Ω), and the period between pulses (567 ns). As shown by the horizontal dashed lines in Fig. 5, the average and the standard deviations of the current ratio values are 1.02 ± 0.07 . Thus within the 7% uncertainty in the measurements, the current ratio is independent of the bias voltage and the incident wavelength. This independence implies that the apparatus used to measure the transient signal and the mathematical model for the transient signal analysis account for the photodiode current with an accuracy of 7%.

Shown in Fig. 6 are the oscilloscope curves, fitted curves, and inferred input pulses for the case of 68-ps laser illumination of the AXUV-HS5 photodiode with a 0.8-mm-diameter aperture (photodiode 1 in Table 1). The applied bias voltages were 22, 44, 66, and 88 V. The derived quantities (area under the curve, curve height, offset time of the input pulse, and photodiode capacitance) for AXUV-HS5 photodiodes with 0.8- and 0.4-mm-diameter apertures (photodiodes 1 and 2 in Table 1) are shown in Fig. 7. The areas

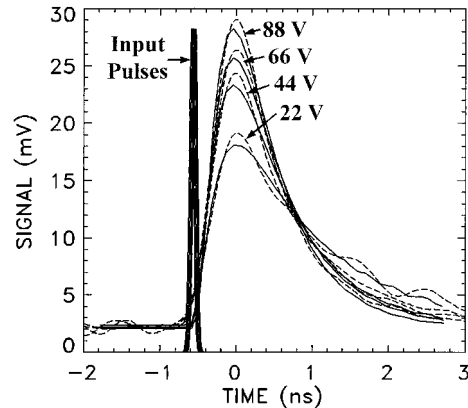


Fig. 6. Observed voltage pulses (dashed curves) and the fitted voltage curves (solid curves) recorded with the AXUV-HS5 photodiodes with a 0.8-mm aperture, 68-ps laser illumination, and bias voltages of 88, 66, 44, and 22 V. The inferred input pulses are also shown.

increase by approximately 10% with increasing bias voltage; this increase may result from saturation of the photodiode under intense laser illumination and the extension of the linear response range with increasing bias voltage. With bias voltage the curve heights significantly increase and the capacitances (and fall times) decrease. The offset time of the input pulse is in the range of 0.54 to 0.61 ns.

The photodiode capacitance determined with

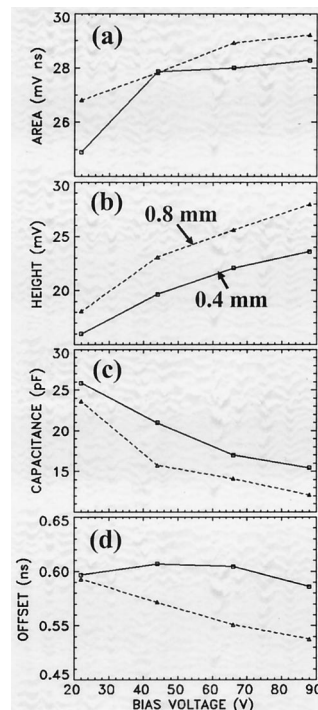


Fig. 7. Fitted parameters for AXUV-HS5 photodiodes and 68-ps pulsed laser illumination. (a) Area under the voltage signal curve. (b) Height of the voltage signal curve. (c) Photodiode capacitance. (d) Offset time between the peaks of the signal curve and the driving pulse. The aperture sizes were 0.4 (solid curve) and 0.8 mm (dashed curve).

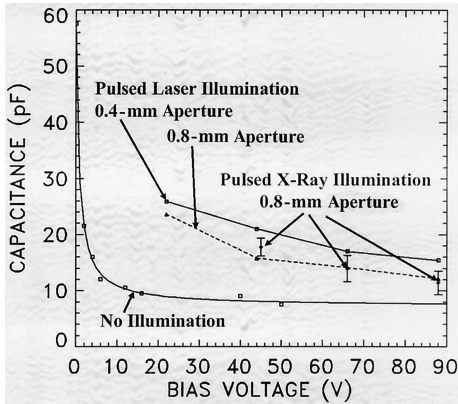


Fig. 8. AXUV-HS5 photodiode capacitance determined with pulsed laser illumination, pulsed x-ray illumination, and no illumination.

pulsed laser and x-ray illumination are compared with the capacitance⁷ determined from the AXUV-HS5 photodiode's electrical response with no illumination in Fig. 8. In the case of pulsed x-ray illumination, the data points are the wavelength-averaged values for the three bias voltages shown in Fig. 4(c), and the error bars are the standard deviations. The capacitance of the AXUV-HS5 photodiode with a 0.8-mm aperture determined by pulsed x-ray illumination and pulsed laser illumination are in good agreement.

In general, the capacitance decreases with bias voltage. This decrease occurs because the width of the depletion region increases with bias voltage, and the decrease in the capacitance with depletion-region width is analogous to the decrease in capacitance of a parallel-plate capacitor when the plate separation increases.⁸ The capacitance is higher with illumination than without illumination because the charge injected into the depletion region by illumination in effect increases the dielectric constant and the capacitance.

By means of the model of the photodiode response to pulsed illumination, calculated signal curves are

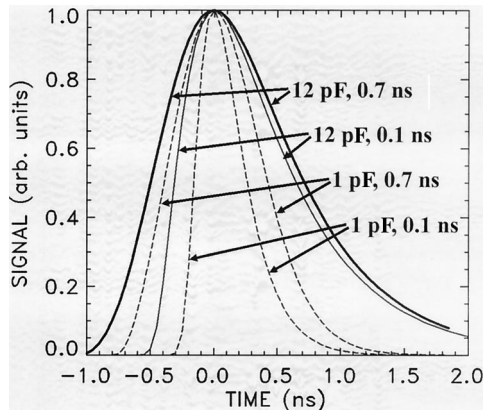


Fig. 9. Calculated photodiode signal curves for the indicated values of photodiode capacitance (1 or 12 pF) and input pulse fwhm duration (0.1 or 0.7 ns).

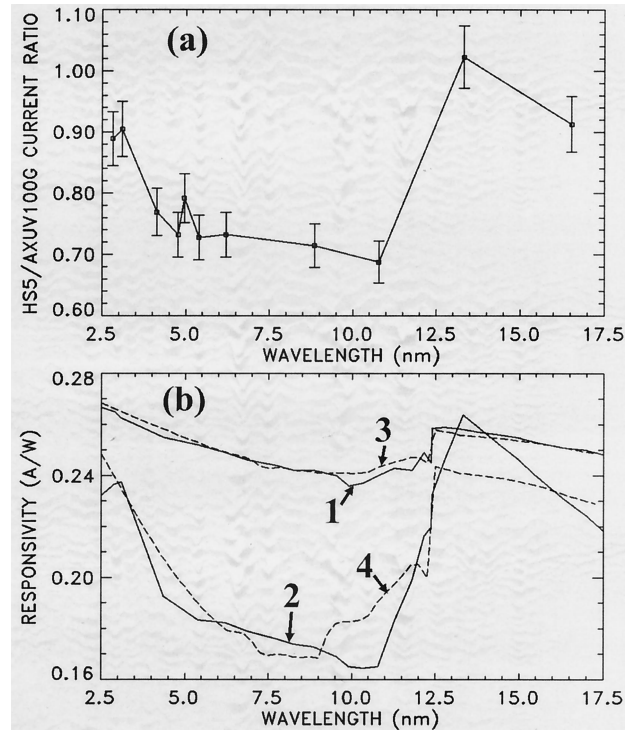


Fig. 10. (a) Ratio of the time-averaged currents from the AXUV-HS5 and the AXUV-100G photodiodes where $\pm 5\%$ error bars are indicated. (b) The measured responsivities for the AXUV-100G (curve 1) and the AXUV-HS5 (curve 2) photodiodes. The calculated responsivities of the AXUV-100G (curve 3) and the AXUV-HS5 (curve 4) photodiodes.

shown in Fig. 9 for the indicated values of photodiode capacitance (1 or 12 pF) and of input pulse FWHM duration (0.1 or 0.7 ns). The voltage amplifier and the oscilloscope were assumed to have 1-GHz band-passes. These curves illustrate the effects of capacitance and of input pulse duration on the fall and the rise times. The fall times are influenced primarily by capacitance and less by input pulse duration. The rise times increase with input pulse duration and capacitance.

4. Absolute Responsivity

The absolute responsivity of the AXUV-HS5 photodiode was determined by comparison with the AXUV-100G reference photodiode, both with 0.8-mm-diameter apertures (photodiodes 1 and 4 in Table 1). The time-averaged currents were measured by the Keithley electrometers, and the current ratios are shown in Fig. 10(a) where $\pm 5\%$ error bars are indicated.

The AXUV-HS5 responsivity was determined by multiplication of the current ratio by the previously determined absolute responsivity of the AXUV-100G reference photodiode.¹⁰ In Fig. 10(b), curve 1 is the AXUV-100G responsivity and curve 2 is the AXUV-HS5 responsivity derived from the current ratio. The AXUV-HS5 has relatively low responsivity at wavelengths shorter than the silicon L absorption edge at 12.4 nm where silicon is absorptive. A sim-

ilar decrease in responsivity was observed for another silicon photodiode.¹¹ With a responsivity model that accounted for the penetration of the incident radiation through the surface dead layer and into the depletion region and the carrier collection efficiencies (CCEs) in the various photodiode regions, the low responsivity was attributed to unusually low CCE (15%) in the depletion region.¹¹ An alternate explanation of the low responsivity at wavelengths shorter than the silicon L edge, that of increased thickness of the SiO₂ surface dead layer, did not accurately model the data.

The responsivity model of Ref. 11 was utilized to analyze the responsivity of the AXUV-HS5 photodiode. As discussed in more detail in Ref. 11, the responsivity model calculates the electromagnetic field as a function of depth into the various regions of the device. The model accounts for the reflectance and transmittance at each boundary and the attenuation of the field strength in each region of the device. The calculated responsivity, the current in the external circuit divided by the incident radiation power, depends only on the optical properties and the CCEs in the regions of the device. As discussed in Ref. 11, the optical properties were derived from the compilations of Refs. 12–15.

The modeled regions are the following: (i) 6-nm-thick SiO₂ surface layer, (ii) 100-nm-thick phosphorous-doped (P-doped) silicon, (iii) 0.15- μ m-thick silicon, and (iv) >25- μ m-thick silicon. For each region, the model calculates the energy deposition based on the attenuation of the electromagnetic field and the collected charge based on the electron-hole pair creation energy (3.64 eV/pair) and the assumed CCE. The photodiode responsivity is the total current collected from all regions divided by the incident radiation power. The only free parameters in the calculation are the CCE assumed in each region. It is known that the CCE in the surface layer is very small and that the CCE in the depletion region is nearly 100%.⁷ Within these bounds, the CCE in each region was varied so that the calculated responsivity was in good agreement with the measured absolute responsivity of the AXUV-100G photodiode. The CCE values in the four photodiode regions that gave the best agreement with the measurements are the following: (i) 15%, (ii) 95%, (iii) 99%, and (iv) 100%. Thus the CCE in the SiO₂ surface layer is 15%, and the CCE increases rapidly to 100% in the underlying silicon regions. The calculated responsivity, curve 3 in Fig. 10(b), is in excellent agreement with the measured responsivity, curve 1.

The calculated responsivities from each of the four AXUV-100G photodiode regions, the current collected from the region divided by the radiation power incident on the surface of the photodiode, are shown in Fig. 11(a) by curves 1 through 4. Curve 5 is the total responsivity and is in good agreement with the measured absolute responsivity (data points). The responsivity from the 6-nm surface SiO₂ layer (curve 1) is very small owing to the small layer thickness and low CCE. For wavelengths shorter than the

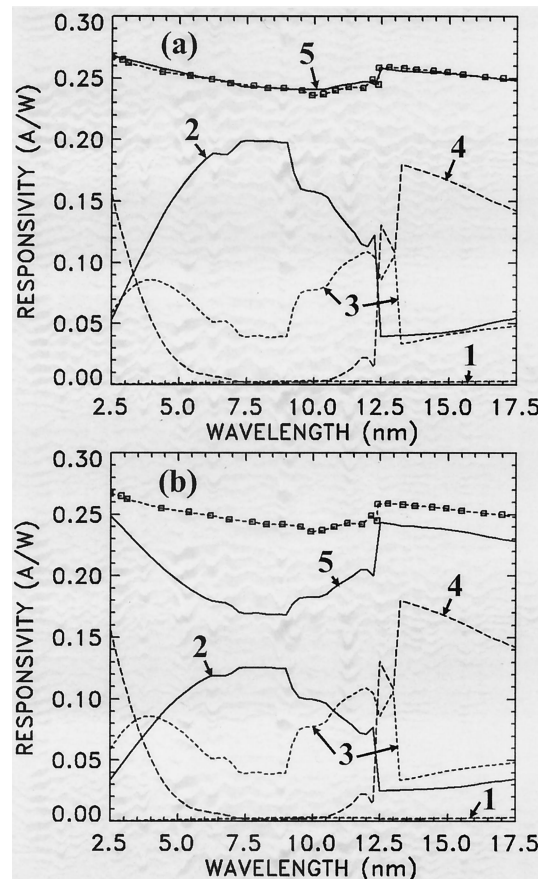


Fig. 11. Curves 1 through 4 are the calculated responsivities from each of the four photodiode regions of the AXUV-100G photodiode (a) and the AXUV-HS5 photodiode (b). Curve 5 is the total responsivity, and the data points are the measured absolute responsivity of the AXUV-100G photodiode from Ref. 10.

silicon L edge at 12.4 nm, where silicon is relatively absorptive, the responsivity from the underlying 100-nm, P-doped silicon region (curve 2) is large. At wavelengths longer than 12.4 nm, where silicon is relatively transmissive, the responsivity is highest in the thicker underlying silicon regions (curves 3 and 4). Thus the total calculated responsivity of the device depends primarily on the assumed CCE in the P-doped region for wavelengths shorter than 12.4 nm and on the CCE in the underlying silicon regions for wavelengths longer than 12.4 nm.

The same computation model was applied to the AXUV-HS5 photodiode with a measured responsivity, relative to the AXUV-100G, given by curve 2 in Fig. 10(b). The calculated responsivity is shown by curve 4 in Fig. 10(b), and the responsivities from the various layers are shown in Fig. 11(b). The derived CCE in the four AXUV-HS5 regions are the following: (i) 15%, (ii) 60%, (iii) 99%, and (iv) 100%. The measured and calculated AXUV-HS5 responsivities are shown by curves 2 and 4 in Fig. 10(b), respectively.

The relatively low AXUV-HS5 responsivity for wavelengths shorter than 12.4 nm is attributed to the low CCE (60%) in the P-doped region. The low responsivity at less than 12.4 nm could not be explained

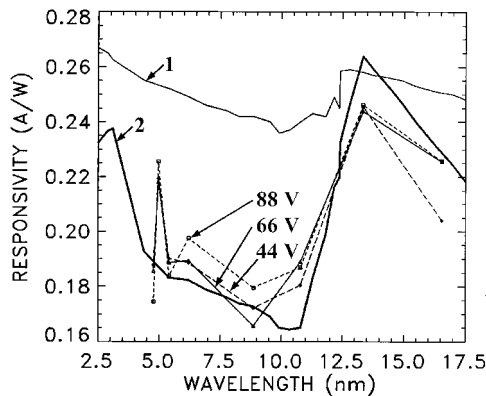


Fig. 12. Steady-state responsivities of the AXUV-100G reference photodiode (curve 1) and the AXUV-HS5 photodiode (curve 2) without bias voltage. The other three curves are the responsivities of the AXUV-HS5 in the pulsed mode with bias voltages of 44, 66, and 88 V.

by an unexpectedly thick SiO₂ surface layer. Assuming an increased thickness of the SiO₂ surface layer resulted in a much smaller jump in responsivity at the silicon L edge and in responsivity at wavelengths shorter than 5 nm that was too high. Thus assuming a thicker SiO₂ surface layer does not accurately fit the AXUV-HS5 responsivity data.

The origin of the unexpectedly low CCE and responsivity for wavelengths shorter than 12.4 nm requires further investigation. It is possible that the AXUV-HS5 had intrinsically low CCE in the P-doped region or that the AXUV-HS5 may have suffered radiation damage that reduced the CCE.

The responsivity of the AXUV-HS5 photodiode in the pulsed mode with applied bias voltage and a 0.8-mm aperture (photodiode 1 in Table 1) was derived from its equivalent transient current and from the incident radiation flux as measured by the AXUV-100G reference photodiode with a 0.8-mm aperture (photodiode 4 in Table 1). As discussed in Section 3, the AXUV-HS5 equivalent current is the integrated area under the oscilloscope curve, shown in Fig. 4(a), divided by the amplifier gain (680), the resistance (50 Ω), and the period between pulses (567 ns). The incident radiation flux is the AXUV-100G current divided by the measured absolute responsivity from Ref. 10 (data points in Fig. 11 and curve 1 in Fig. 12). The AXUV-HS5 responsivity in the pulsed mode with bias voltages of 44, 66, and 88 V are shown in Fig. 12 and are in agreement, within the uncertainty in the measurements, with the steady-state AXUV-HS5 responsivity without bias voltage (curve 2 in Fig. 10 and curve 2 in Fig. 12). In addition, the AXUV-HS5 responsivity in the pulsed mode is independent of the bias voltage.

These results imply that throughout the 4- to 16-nm wavelength range of study the charge swept out by the bias voltage and collected in the pulsed mode is independent of the bias voltage and is equivalent to the charge collected in the steady-state mode without bias voltage. As previously noted, the

AXUV-HS5 responsivity is significantly lower than the responsivity of the AXUV-100G reference photodiode at wavelengths shorter than the silicon L absorption edge at 12.4 nm.

5. Discussion

With pulsed synchrotron radiation in the 4- to 16-nm-wavelength range, the capacitance of the 1-mm² silicon photodiode (type AXUV-HS5) was found to decrease with increasing bias voltage and to be fairly independent of wavelength. The capacitance determined with pulsed laser radiation and similar bias voltages was in good agreement with the capacitance determined with pulsed synchrotron radiation. This implies that energy deposition depth and transient time effects, which may differ depending on the radiation wavelength, are not significant for the photodiode under study. Since the capacitance determined with pulsed laser radiation is valid for x-ray and EUV wavelengths, it is not necessary to use x-ray and EUV radiation to characterize the expected time response in those wavelength regions.

The accuracies of the signal analysis and the inferred quantities such as photodiode capacitance were generally near the ±10% level. The mathematical model for the response of the photodiode to pulsed irradiation can be used to predict the time-dependent response of the AXUV-HS5 photodiode. The response depends on the photodiode capacitance, the width and shape of the input radiation pulse, and the bandpass of the measurement apparatus. Conversely, if one knows the photodiode capacitance, for example, from pulsed laser measurements, the time dependence of the input driving pulse can be determined for wide-ranging incident wavelengths (including x-ray and EUV wavelengths as shown in Fig. 3).

The responsivities of the AXUV-HS5 photodiode in the steady-state mode (without bias voltage) and in pulsed mode (with bias voltage) were found to be the same, within the uncertainties in the measurements, and were significantly lower than the responsivity of a AXUV-100G reference photodiode for wavelengths shorter than the silicon L absorption edge at 12.4 nm. Using a computational model for the responsivities of the two photodiodes, it was found that the low AXUV-HS5 responsivity could be explained by an unexpectedly low CCE in the P-doped region, 60% compared with the expected 95%. Although the two photodiodes were fabricated by use of similar lithographic processes, the AXUV-HS5 may have intrinsically lower responsivity than the AXUV-100G for wavelengths shorter than 12.4 nm, or the AXUV-HS5 may have suffered radiation damage. In any case, to use the AXUV-HS5 for absolutely calibrated measurements of radiation fluxes in the x-ray and EUV wavelength ranges, one must measure the AXUV-HS5 absolute responsivity in these wavelength ranges.

The two computational models, for the absolute responsivity and the time response, could be combined to determine the origin of the capacitance values as functions of bias voltage and incident

wavelength. This would require more detailed knowledge of the various diode regions' physical characteristics and of the electrical connections to the device. In particular, the dynamic effects of the carrier drift velocities, the width of the depletion region, and the injected charge would need to be considered.

This research was supported by the Naval Research Laboratory NIKE laser program through the Department of Energy. The National Synchrotron Light Source is supported by the Department of Energy. J. Trewin provided physical insight for the interpretation of the results.

References

1. J. Weaver, G. Holland, U. Feldman, J. Seely, C. Brown, V. Serlin, A. Deniz, and M. Klapisch, "The determination of absolutely calibrated spectra from laser produced plasmas using a transmission grating spectrometer at the NIKE laser facility," *Rev. Sci. Instrum.* **72**, 108–118 (2001).
2. R. T. Eagleton and L. E. Ruggles, "Soft x-ray characterization of a silicon p–n photodiode using a laser produced plasma source," *Rev. Sci. Instrum.* **72**, 1205 (2001).
3. L. R. Canfield, "Photodiode Detectors," in *Vacuum Ultraviolet Spectroscopy II*, J. A. R. Samson and D. L. Ederer, eds. (Academic, San Diego, 1998).
4. J. C. Rife, H. R. Sadeghi, and W. R. Hunter, "Upgrades and recent performance of the grating/crystal monochromator," *Rev. Sci. Instrum.* **60**, 2064–2067 (1989).
5. W. R. Hunter and J. C. Rife, "An ultrahigh vacuum reflectometer/goniometer for use with synchrotron radiation," *Nucl. Instrum. Methods A* **246**, 465–468 (1986).
6. E. Z. Rothman, ed., National Synchrotron Light Source Activity Report, Brookhaven National Laboratory publication BNL-52554 (Brookhaven National Laboratory, Brookhaven, N.Y., 1998), pp. 4–9.
7. International Radiation Detectors Inc., 2527 West 237 Street, Unit C, Torrance, Calif. 90505; www.ird-inc.com.
8. G. W. Neudeck, *The PN Junction Diode* (Addison-Wesley, Reading, Pa., 1989).
9. J. Millman and C. Halkias, *Integrated Electronics: Analog and Digital Circuits and Systems* (McGraw-Hill, New York, 1972).
10. F. Scholze, H. Rabus, and G. Ulm, "Measurement of the mean electron–hole pair creation energy in crystalline silicon for photons in the 50–1500 eV spectral range," *Appl. Phys. Lett.* **69**, 2974–2976 (1996).
11. J. F. Seely, "Responsivity model for a silicon photodiode in the extreme ultraviolet," in *Instrumentation for UV/EUV Astronomy and Solar Missions*, S. Fineschi, C. Korendyke, O. Siegmund, and B. Woodgate, eds., *Proc. SPIE* **4139**, 1–7 (2000).
12. B. L. Henke, E. M. Gullikson, and J. C. Davis, "X-ray interactions: photoabsorption, scattering, transmission, and reflection at $E = 50$ – $30,000$ eV, $Z = 1$ – 92 ," *At. Data Nucl. Data Tables* **54**, 181–342 (1993).
13. Updated optical constants were obtained from the internet site (retrieved June 2000), cindy.lbl.gov/optical_constants.
14. D. F. Edwards, "Silicon (Si)," in *Handbook of Optical Constants of Solids*, E. D. Palik, ed. (Academic, San Diego, 1985), pp. 547–569.
15. H. R. Philipp, "Silicon dioxide (SiO₂)," in *Handbook of Optical Constants of Solids*, E. D. Palik, ed. (Academic, San Diego, 1985), pp. 719–747.